

Optics in the Schwarzschild spacetime

Andrej Čadež* and Uroš Kostić

Department of Physics, Faculty of Mathematics and Physics, University of Ljubljana, Jadranska 19, 1000 Ljubljana, Slovenia
(Received 29 June 2005; published 28 November 2005)

Realistic modeling of radiation transfer in and from variable accretion disks around black holes requires the solution of the problem: find the constants of motion and equation of motion of a lightlike geodesic connecting two arbitrary points in space. Here we give the complete solution of this problem in the Schwarzschild spacetime.

DOI: [10.1103/PhysRevD.72.104024](https://doi.org/10.1103/PhysRevD.72.104024)

PACS numbers: 04.20.Jb, 04.25.Dm, 95.30.Sf

I. INTRODUCTION

The first light detected from a relativistic region about a black hole was discovered by the ASCA satellite [1,2]. The now accepted theoretical model describing the broad x-ray emission lines is that of an accretion disk around either a Kerr or a Schwarzschild black hole [3–10]. This discovery increased the interest for phenomena occurring in the vicinity of black holes. We now know that other interesting high energy phenomena, such as x-ray flares [11,12] or quasiperiodic oscillations [13,14] are occurring in the environment of black holes. To further the understanding of such phenomena from the theoretical point of view, it is important to develop tools to model the phenomena themselves as well as to model radiation transfer in and from these strongly curved regions of spacetime.

Most current accretion disk models are very simple from the radiation transfer point of view. They consider disks as geometrically thin and optically thick. Light that reaches a far observer comes directly (without being scattered) from a very definite point on the disk. Therefore, line profiles can be calculated by aiming lightlike geodesic from a point on the disk to the observer or vice versa, aiming from the observer to points on the disk. In such ray-tracing procedures geodesic equations are usually solved by direct numerical integration [15–17]. However, when modeling transient phenomena produced by small debris around black holes, or by other transient phenomena in the disk (moving hot spots, varying external illumination, waves), it becomes necessary to solve a more difficult radiation transfer problem, the problem of following a single photon through its more than one scattering and/or more than one possible path from the source to the eye of the observer [18,19]. The problem is further complicated by noting that photon arrival times from the same initial source to the observer may (and often will) be markedly different for photons reaching the observer along different possible paths. It is obvious that a multiple scattering path cannot be effectively constructed by aiming geodesics between successive scattering points as the number of successive iterations required would soon blow up. The solution to the

radiation transfer problem thus requires one to be able to follow a light ray from one to the other scattering point along its path. Thus, one would like to find the quickest way to determine all constants of motion of a geodesic that connects the given initial and final point. In this article we give analytic expressions which completely solve this problem in the Schwarzschild spacetime. We also turn this analytic tool into a numerical code and demonstrate that it is much faster, more accurate and more transparent than aiming and integrating geodesic equations. This tool thus opens the possibility to solve complex radiation transfer problems in curved spacetime using similar Monte Carlo techniques that are used in solving radiation problems in flat spacetime.

Our work starts with the results of Chandrasekhar [20] and Rauch and Blandford [21], who expressed the solutions to geodesic equations in terms of elliptic integrals. By inverting their expressions into Jacobi elliptic functions [9], we obtain simple solutions for all three types of orbit equations that occur in Schwarzschild spacetime. These solutions no longer contain branch ambiguities. Since these orbits are essentially planar, their equations depend only on two nontrivial constants of motion: the angular momentum and the longitude of the periastron. Expressing the orbit equation at the initial and final points on the geodesic, one obtains two nonlinear equations for the two nontrivial constants of motion. However, since the longitude of the periastron occurs only linearly as the argument of elliptic functions, it is possible to use the elliptic functions addition theorem to eliminate the longitude of the periastron and obtain a single nonlinear equation for the angular momentum as a function of initial and final coordinates. Here we derive these equations for all three types of orbits and discuss their properties and solutions. We also write down all the other constants of motion in terms of final and initial point coordinates and give analytic expressions for travel times.

II. CONNECTING TWO POINTS WITH A LIGHTLIKE GEODESIC

In the Schwarzschild spacetime it is customary to introduce Schwarzschild coordinates t , r , θ and φ . In these coordinates geodesics are governed by the Hamiltonian

*Electronic address: andrej.cadez@fmf.uni-lj.si

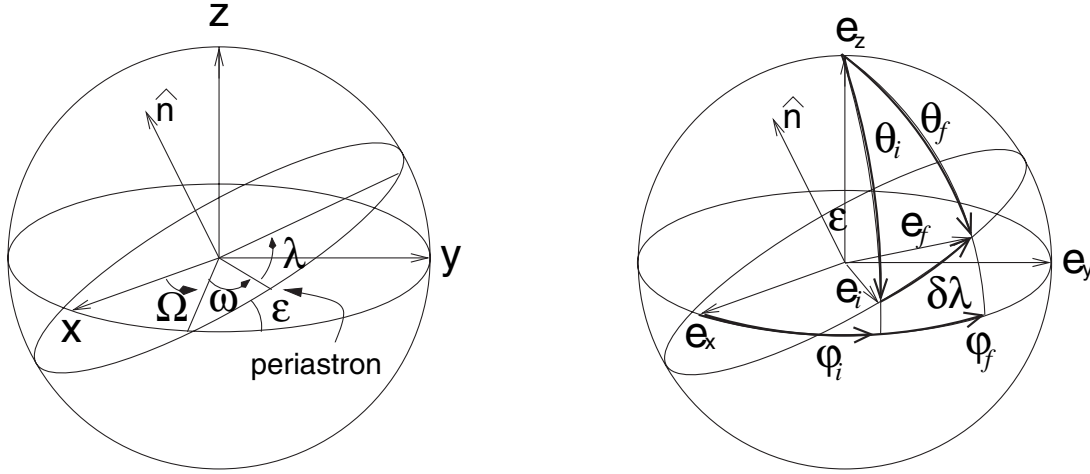


FIG. 1. Left panel: The orbital plane in equatorial coordinates: \hat{n} unit normal, ε inclination, Ω longitude of the ascending node, ω longitude of the periastron and λ the true anomaly. Right panel: The initial $\mathcal{P}_i = (\theta_i, \varphi_i)$ and the final $\mathcal{P}_f = (\theta_f, \varphi_f)$ points.

$$H = \frac{1}{2} \left[-\frac{1}{1 - \frac{2M}{r}} p_t^2 + \left(1 - \frac{2M}{r}\right) p_r^2 + \frac{1}{r^2} \left(p_\theta^2 + \frac{1}{\sin^2 \theta} p_\varphi^2 \right) \right], \quad (1)$$

which admits 8 constants of motion: the value of the Hamiltonian (H) and the value of the Lagrangian (L) (the ratio of the two defining the relation between time and proper time), the energy $E = p_t$, the angular momentum (\vec{l}), the longitude of the periastron (ω) and the time of periastron passage (for Hamiltonian and Poisson bracket formalism see Goldstein [22]).

The angular momentum is expressed as $\vec{l} = l \cdot \hat{n}$, where \hat{n} is the unit vector along \vec{l} , which is defined by the inclination of the orbit (ε) and the longitude of the ascending node (Ω).

Consider a lightlike geodesic connecting the initial point \mathcal{P}_i and the final point \mathcal{P}_f . Five constants $H = 0$, $L = 0$, E , Ω and ε are determined readily. So one can use the true anomaly λ as a parameter along the geodesic. From the initial to the final point λ increases by

$$\Delta \lambda_f = \delta \lambda + 2\pi k, \quad (2)$$

where

$$\delta \lambda = \arccos[\cos \theta_i \cos \theta_f + \sin \theta_i \sin \theta_f \cos(\varphi_f - \varphi_i)], \quad (3)$$

and the winding number $k = \dots - 1, 0, 1, \dots$ tells how many times a geodesic winds around the black hole.¹

The two constants Ω and ε are obtained from angular coordinates of the initial and final points (see Fig. 1) with the help of basic spherical trigonometry [23]:

$$\cos \varepsilon = \frac{\sin \theta_i \sin \theta_f \sin(\varphi_f - \varphi_i)}{\sin \delta \lambda}, \quad (4)$$

$$\tan \frac{\Omega}{2} = \frac{\sin \theta_i \cos \theta_f \sin \varphi_i - \cos \theta_i \sin \theta_f \sin \varphi_f}{\sin \varepsilon \sin \delta \lambda + \sin \theta_i \cos \theta_f \cos \varphi_i - \cos \theta_i \sin \theta_f \cos \varphi_f}. \quad (5)$$

Since the variable λ is conjugate to the orbital angular momentum, it obeys the Poisson bracket relation $[\lambda, l] = 1$, so that the angles θ and φ are expressed with λ as follows [24] [Eqs. (6)–(16)]:

$$\cos \theta = -\sin \varepsilon \sin(\lambda + \omega), \quad (6)$$

$$\tan \frac{\varphi - \Omega}{2} = \frac{\cos \varepsilon \sin(\lambda + \omega)}{\sin \theta + \cos(\lambda + \omega)} \quad (7)$$

and² the differential equation for orbits of lightlike geodesics becomes

$$\frac{du}{d\lambda} = \pm \sqrt{a^2 - u^2(1 - u)}. \quad (8)$$

Here $u = 2M/r$ and $a = 2ME/l$. The solutions to this equation, called orbit equations, depend only on the parameter a and are of three types (Fig. 2):

- (i) *type A*.—scattering orbits with both end points at infinity; their angular momentum parameter is on the interval $0 < a < 2/3\sqrt{3}$. Scattering orbits can never extend below $r = 3M$;
- (ii) *type B*.—plunging orbits with one end at infinity and the other behind the horizon, $a > 2/3\sqrt{3}$;

¹Note, if $\Delta \lambda_f < 0$, replace $\Delta \lambda_f \rightarrow -\Delta \lambda_f$ and $\hat{n} \rightarrow -\hat{n}$.

²Note that $\sin \theta = +\sqrt{1 - \cos^2 \theta}$.

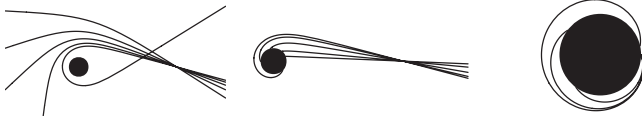


FIG. 2. Left: Some orbits of type A with parameters $r_i = 20M$ and $a_{\text{crit}} - a \in \{0.2, 0.15, 0.1, 0.05, 0.005\}$. Middle: Orbits of type B with parameters $r_i = 20M$ and $a - a_{\text{crit}} \in \{2, 0.7, 0.2, 0.05, 0.005\}$. Right: Orbits of type C with parameters $r_i = 2.00001M$ and $a_{\text{crit}} - a \in \{0.01, 0.005, 0.001\}$. The radius of the black circle is the Schwarzschild radius.

(iii) *type C*.—near orbits with both ends behind the horizon of the black hole; their angular momentum parameter is on the interval $0 < a < 2/3\sqrt{3}$. Near orbits can never reach beyond $r = 3M$.

For completeness, we list the solutions of the orbit equation (8) in terms of a few auxiliary parameters.

Type A

Introduce $a = (2/3\sqrt{3}) \sin \frac{\psi}{2}$ ($0 < \psi < \pi$) and the following auxiliary parameters, functions of ψ only:

$$u_1 = \frac{1}{3} \left(1 + 2 \cos \frac{\psi}{3} \right), \quad (9a)$$

$$u_2 = \frac{1}{3} \left(1 + 2 \cos \frac{\psi - 2\pi}{3} \right), \quad (9b)$$

$$u_3 = \frac{1}{3} \left(1 + 2 \cos \frac{\psi + 2\pi}{3} \right), \quad (9c)$$

$$m = \frac{u_2 - u_3}{u_1 - u_3}, \quad (9d)$$

$$n = \frac{2}{\sqrt{u_1 - u_3}}, \quad (9e)$$

$$\chi_i \text{ such that } u_i = u_2 - (u_2 - u_3) \cos^2 \chi_i, \quad (9f)$$

where $u_i = 2M/r_i$ and similarly $u_f = 2M/r_f$. In terms of these, the type A differential equation for the orbit becomes (Fig. 2, left)

$$u = u_2 - (u_2 - u_3) \text{cn}^2 \left(F(\chi_i | m) + \frac{\Delta\lambda}{n} | m \right), \quad (10)$$

with $\Delta\lambda = \lambda - \lambda_i$ and $\Delta\lambda/n \in \{x_{\min} - x_i, (2K(m) - x_{\min}) - x_i\}$, where $x_{\min} = F(\arccos \sqrt{u_2/(u_2 - u_3)} | m)$ and $x_i = F(\arccos \sqrt{(u_2 - u_i)/(u_2 - u_3)} | m)$. Here F and K are the incomplete and complete elliptic integrals of the first kind [25].

Critical A

A special limiting case of solution (10) for $\psi = \pi$ ($a = 2/3\sqrt{3}$) and $u_i < 2/3$ ($r_i > 3M$) is

$$u = -\frac{1}{3} + \tanh^2 \left(\text{artanh} \sqrt{u_i + 1/3} + \frac{\Delta\lambda}{2} \right), \quad (11)$$

with $\Delta\lambda = \lambda - \lambda_i$ and $\Delta\lambda \in \{2 \text{artanh} \sqrt{1/3} - 2 \text{artanh} \sqrt{u_i + 1/3}, \infty\}$.

Type B

Introduce $a = (2/3\sqrt{3}) \cosh \mu$ ($0 < \mu < \infty$) and the auxiliary parameters, functions of μ only:

$$u_1 = \frac{1}{3} \left(1 - 2 \cosh \frac{2\mu}{3} \right), \quad (12a)$$

$$m = \frac{1}{2} \left(1 - \frac{3u_1 - 1}{2\sqrt{u_1(3u_1 - 2)}} \right), \quad (12b)$$

$$n = (u_1(3u_1 - 2))^{-1/4}, \quad (12c)$$

$$\chi_i \text{ such that } u_i = u_1 + \frac{1}{n^2} \frac{1 - \cos \chi_i}{1 + \cos \chi_i}. \quad (12d)$$

The type B differential equation for the orbit is (Fig. 2, middle)

$$u = u_1 + \frac{1}{n^2} \frac{1 - \text{cn}(F(\chi_i | m) + \frac{\Delta\lambda}{n} | m)}{1 + \text{cn}(F(\chi_i | m) + \frac{\Delta\lambda}{n} | m)}, \quad (13)$$

with $\Delta\lambda = \lambda - \lambda_i$ and $\Delta\lambda/n \in \{F(\chi_{BH} | m) - F(\chi_i | m), F(\chi_\infty | m) - F(\chi_i | m)\}$, where $\chi_{BH} = \arccos[(1 - n^2(1 - u_1))/(1 + n^2(1 - u_1))]$ and $\chi_\infty = \arccos[(1 + n^2 u_1)/(1 - n^2 u_1)]$.

Type C

Introduce $a = (2/3\sqrt{3}) \sin(\psi/2)$ ($0 < \psi < \pi$) and the auxiliary parameters, functions of ψ only:

$$u_1 = \frac{1}{3} \left(1 + 2 \cos \frac{\psi}{3} \right), \quad (14a)$$

$$u_2 = \frac{1}{3} \left(1 + 2 \cos \frac{\psi - 2\pi}{3} \right), \quad (14b)$$

$$u_3 = \frac{1}{3} \left(1 + 2 \cos \frac{\psi + 2\pi}{3} \right), \quad (14c)$$

$$m = \frac{1}{2} \left(1 - \frac{u_1 - (u_2 + u_3)/2}{\sqrt{(u_1 - u_3)(u_1 - u_2)}} \right), \quad (14d)$$

$$n = ((u_1 - u_2)(u_1 - u_3))^{-1/4}, \quad (14e)$$

$$\chi_i \text{ such that } u_i = u_1 + \frac{1}{n^2} \frac{1 - \cos \chi_i}{1 + \cos \chi_i}. \quad (14f)$$

The type C differential equation for the orbit is (Fig. 2, right)

$$u = u_1 + \frac{1}{n^2} \frac{1 - \text{cn}(F(\chi_i | m) + \frac{\Delta\lambda}{n} | m)}{1 + \text{cn}(F(\chi_i | m) + \frac{\Delta\lambda}{n} | m)}, \quad (15)$$

with $\Delta\lambda = \lambda - \lambda_i$ and $\Delta\lambda/n \in \{-F(\chi_{BH} | m) - F(\chi_i | m), F(\chi_{BH} | m) - F(\chi_i | m)\}$, where $\chi_{BH} = \arccos[(1 - n^2(1 - u_1))/(1 + n^2(1 - u_1))]$.

Critical C

A special limiting case of the solution of (15) for $\psi = \frac{\pi}{2}$ ($a = 2/3\sqrt{3}$) and $u_i > 2/3$ ($r_i < 3M$) is

$$u = -\frac{1}{3} + \coth^2\left(\operatorname{arcoth}\sqrt{u_i + 1/3} + \frac{\Delta\lambda}{2}\right), \quad (16)$$

with $\Delta\lambda = \lambda - \lambda_i$ and $\Delta\lambda \in \{2 \operatorname{arcoth}\sqrt{4/3} - 2 \operatorname{arcoth}\sqrt{u_i + 1/3}, \infty\}$.

The two constants of motion ω and a can now be determined in two steps. First we determine the type of the orbit following reasoning illustrated in Fig. 3 and then we solve the two equations obtained from the orbit equation at the initial and the final points [26–29].

We note that the parameter ω appears in a contrived form as the starting point of the true anomaly only in the argument of the Jacobi functions, therefore, it can be eliminated from the two equations by using the Jacobi elliptic functions addition theorem. Let $v = F(\chi_i | m) +$

$\Delta\lambda/n$ be the argument of elliptic functions at the final point of the orbit and $z = F(\chi_i | m)$ be the argument of elliptic functions at the initial point of the orbit. Then one can use orbit equations to write

type A:

$$\operatorname{cn}^2(v | m) = \frac{u_2 - u_f}{u_2 - u_3}, \quad (17a)$$

$$\operatorname{sn}^2(v | m) = \frac{u_f - u_3}{u_2 - u_3}, \quad (17b)$$

$$\operatorname{dn}^2(v | m) = \frac{u_1 - u_f}{u_1 - u_3}, \quad (17c)$$

$$\operatorname{cn}^2(z | m) = \frac{u_2 - u_i}{u_2 - u_3}, \quad (17d)$$

$$\operatorname{sn}^2(z | m) = \frac{u_i - u_3}{u_2 - u_3}, \quad (17e)$$

$$\operatorname{dn}^2(z | m) = \frac{u_1 - u_i}{u_1 - u_3}, \quad (17f)$$

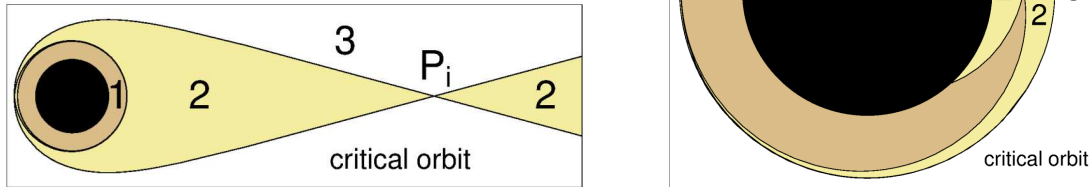


FIG. 3 (color online). For a known initial point \mathcal{P}_i , the two critical orbits through this point divide the orbital plane into three regions. Left panel: initial point at $r > 3M$. If the final point \mathcal{P}_f is in region 3, then all orbits from \mathcal{P}_i are of type A. If \mathcal{P}_f is in region 1, then all orbits from \mathcal{P}_i are of type B. If \mathcal{P}_f is in region 2, then orbits leading to \mathcal{P}_f are of type A if the trajectory winds around the black hole, and of type B if it goes directly from \mathcal{P}_i to \mathcal{P}_f . Right panel: initial point at $r < 3M$. If the final point \mathcal{P}_f is in region 3, then all orbits from \mathcal{P}_i are of type B. If \mathcal{P}_f is in region 1, then orbits from \mathcal{P}_i are of type C. If \mathcal{P}_f is in region 2, then orbits leading to \mathcal{P}_f are of type C if the trajectory winds around the black hole, and of type B if it goes directly from \mathcal{P}_i to \mathcal{P}_f .

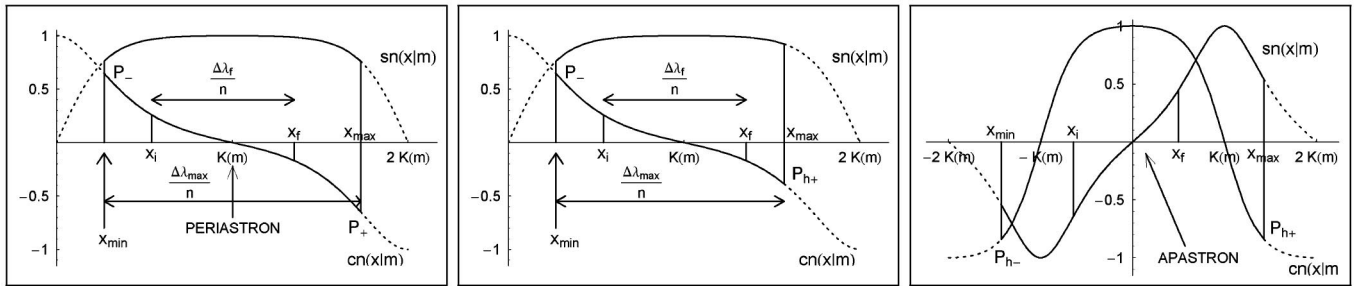


FIG. 4. Functions $\operatorname{cn}(x | m)$ and $\operatorname{sn}(x | m)$ along orbits: left panel, type A; middle panel, type B; right panel, type C. x_{\min} and x_{\max} are at the end points of the orbit and are designated by \mathcal{P}_- and \mathcal{P}_+ if they are at spatial infinity, and \mathcal{P}_{h-} and \mathcal{P}_{h+} if they are at the horizon of the black hole. Interval definitions for the end points follow after Eqs. (10), (13), and (15). $x_i = z$ and $x_f = v$ are at the initial and the final points of the orbit.

types B and C:

$$\text{cn}(v | m) = \frac{1 - n^2(u_f - u_1)}{1 + n^2(u_f - u_1)}, \quad (18a)$$

$$\text{sn}^2(v | m) = \frac{4n^2(u_f - u_1)}{(1 + n^2(u_f - u_1))^2}, \quad (18b)$$

$$\text{dn}^2(v | m) = 1 - \frac{4mn^2(u_f - u_1)}{(1 + n^2(u_f - u_1))^2}, \quad (18c)$$

$$\text{cn}(z | m) = \frac{1 - n^2(u_i - u_1)}{1 + n^2(u_i - u_1)}, \quad (18d)$$

$$\text{sn}^2(z | m) = \frac{4n^2(u_i - u_1)}{(1 + n^2(u_i - u_1))^2}, \quad (18e)$$

$$\text{dn}^2(z | m) = 1 - \frac{4mn^2(u_i - u_1)}{(1 + n^2(u_i - u_1))^2}. \quad (18f)$$

Since $v - z = \Delta\lambda_f/n$ one can use the Jacobi elliptic functions addition theorem to obtain

$$\text{cn}(v - z | m) = \frac{\text{cn}(v | m)\text{cn}(z | m) + \text{sn}(v | m)\text{sn}(z | m)\text{dn}(v | m)\text{dn}(z | m)}{1 - m \text{sn}^2(v | m)\text{sn}^2(z | m)}. \quad (19)$$

This is a nonlinear equation for a (i.e. for ψ or μ with respect to the type of the orbit). Equations (17a)–(17f) and (18a)–(18f), except (18a) and (18d) only give squares, so functions cn and sn are determined only up to the sign; dn is always positive. In order to determine those signs we plot in Fig. 4 the functions sn and cn along orbits together with the interval where the orbit is defined. Figure 4 left panel shows that for type A orbits, only the function cn changes sign at the periastron and the function sn is always positive along the orbit. Thus, the sign of cn is positive if the orbit

did not pass the periastron and negative otherwise. For orbits of type B (Fig. 4 middle panel) sn is always positive, while the sign of cn is determined by (18a) and (18d), thus no sign ambiguity arises. For orbits of type C the sign of cn is again unambiguous [(18a) and (18d)] while the function sn changes sign from negative before apastron to positive after apastron (Fig. 4 right panel). We conclude that the right-hand side of Eq. (19) has two branches if it contains a sign ambiguity. The cases are type A “right₁” and “right₂” and type C “right₁” and “right₃”, where

$$\text{right}_1 = \frac{\text{cn}(v | m)\text{cn}(z | m) + \text{sn}(v | m)\text{sn}(z | m)\text{dn}(v | m)\text{dn}(z | m)}{1 - m \text{sn}^2(v | m)\text{sn}^2(z | m)}, \quad (20)$$

$$\text{right}_2 = \frac{-\text{cn}(v | m)\text{cn}(z | m) + \text{sn}(v | m)\text{sn}(z | m)\text{dn}(v | m)\text{dn}(z | m)}{1 - m \text{sn}^2(v | m)\text{sn}^2(z | m)}, \quad (21)$$

$$\text{right}_3 = \frac{\text{cn}(v | m)\text{cn}(z | m) - \text{sn}(v | m)\text{sn}(z | m)\text{dn}(v | m)\text{dn}(z | m)}{1 - m \text{sn}^2(v | m)\text{sn}^2(z | m)}. \quad (22)$$

In the above the sign of cn or sn is positive when calculated from a square root.

Some examples of determining the value of a are shown in Figs. 5–9. They show the left-hand side and all the appropriate branches of the right-hand side of (19) as a function of ψ or μ for different cases of r_i , r_f and $\Delta\lambda_f$. The solution of Eq. (19), which is the point where “right” crosses “left,” is found numerically by using the Brent

method [30].³ With the now known parameter a it is straightforward to calculate the value of ω [Eqs. (10), (13), and (15)].

³For $\Delta\lambda_f > 2\pi$ there may be more than one solution to the Eq. (19); clearly in this case the orbit is wound about the black hole at $r = 3M$, therefore only the solution with a closest to $2/3\sqrt{3}$ applies.

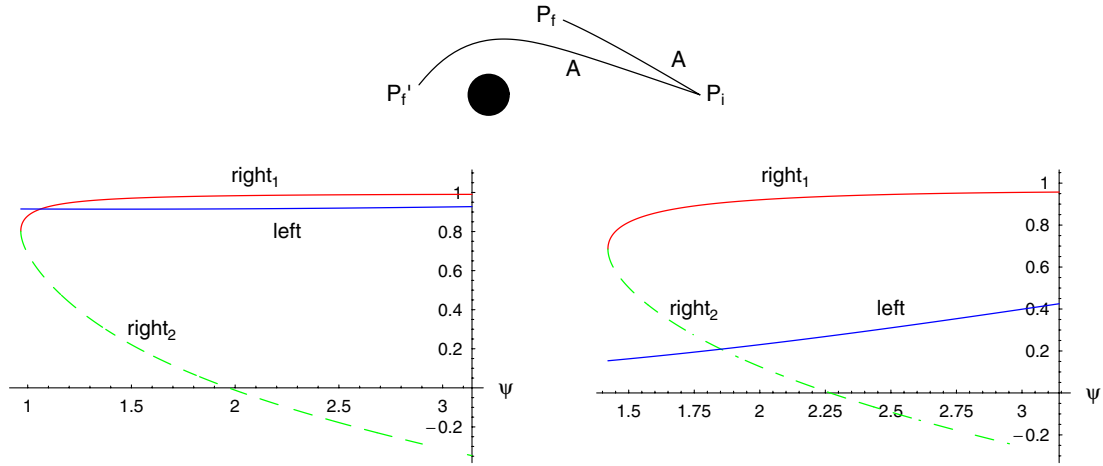


FIG. 5 (color online). Determining the angular momentum parameter for a type A orbit. Left panel: the orbit from \mathcal{P}_i to \mathcal{P}_f does not pass periastron. Right panel: the orbit from \mathcal{P}_i to \mathcal{P}_f passes periastron. The designations right_1 and right_2 refer to the branches (20) and (21) respectively.

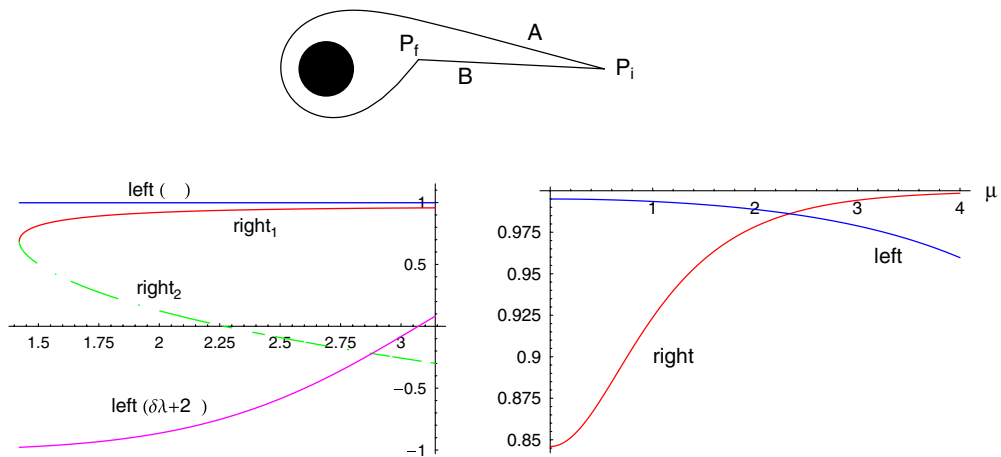


FIG. 6 (color online). Connecting \mathcal{P}_i and \mathcal{P}_f with a type B orbit and a type A winding orbit (winding number $k = 1$); no $k = 0$ type A orbit exists in this case. Left panel: the orbit from \mathcal{P}_i to \mathcal{P}_f of type A. Right panel: the orbit from \mathcal{P}_i to \mathcal{P}_f of type B.

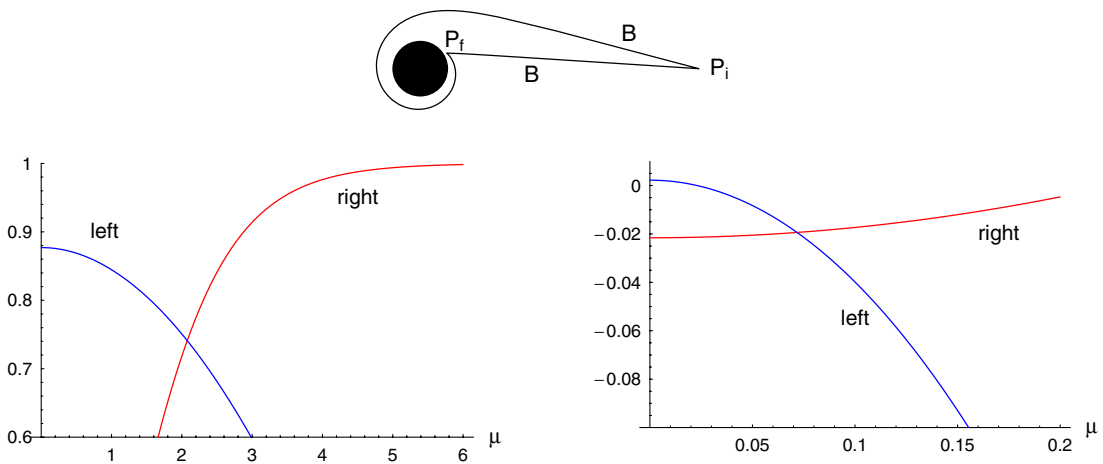


FIG. 7 (color online). Determining the angular momentum parameter for a type B orbit. Left panel: a direct orbit from \mathcal{P}_i to \mathcal{P}_f . Right panel: a winding orbit from \mathcal{P}_i to \mathcal{P}_f (winding number $k = 1$).

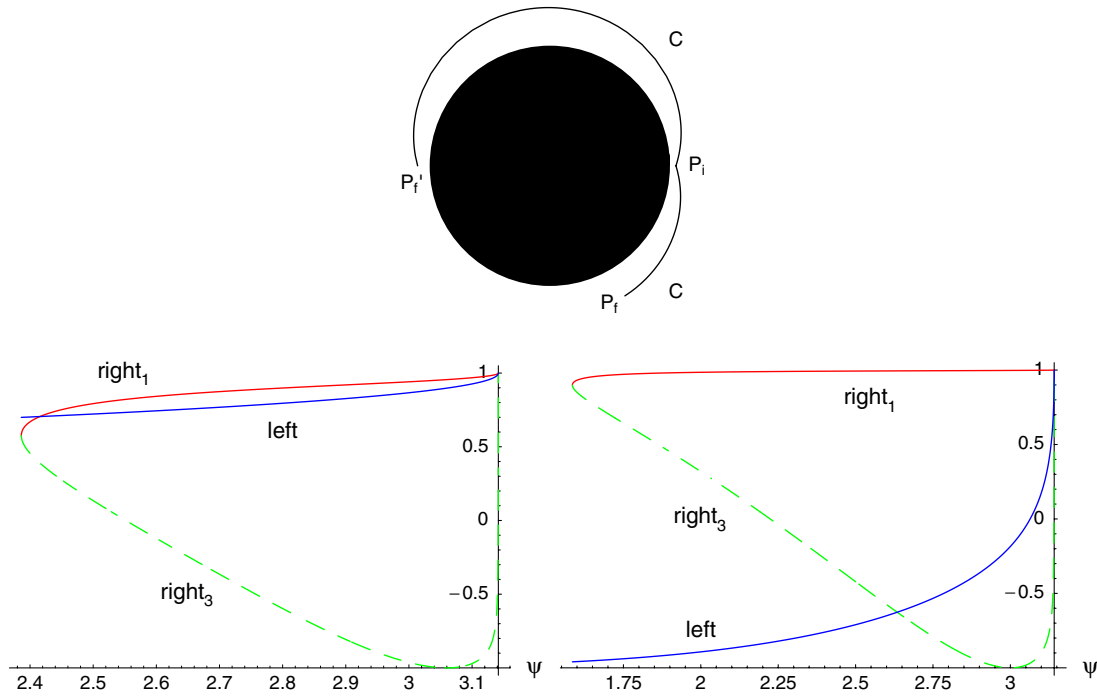


FIG. 8 (color online). Determining the angular momentum parameter for a type C orbit. Left panel: the orbit from \mathcal{P}_i to \mathcal{P}_f does not pass apastron. Right panel: the orbit from \mathcal{P}_i to \mathcal{P}_f passes apastron. The designations right_1 and right_3 refer to the branches (20) and (22) respectively.

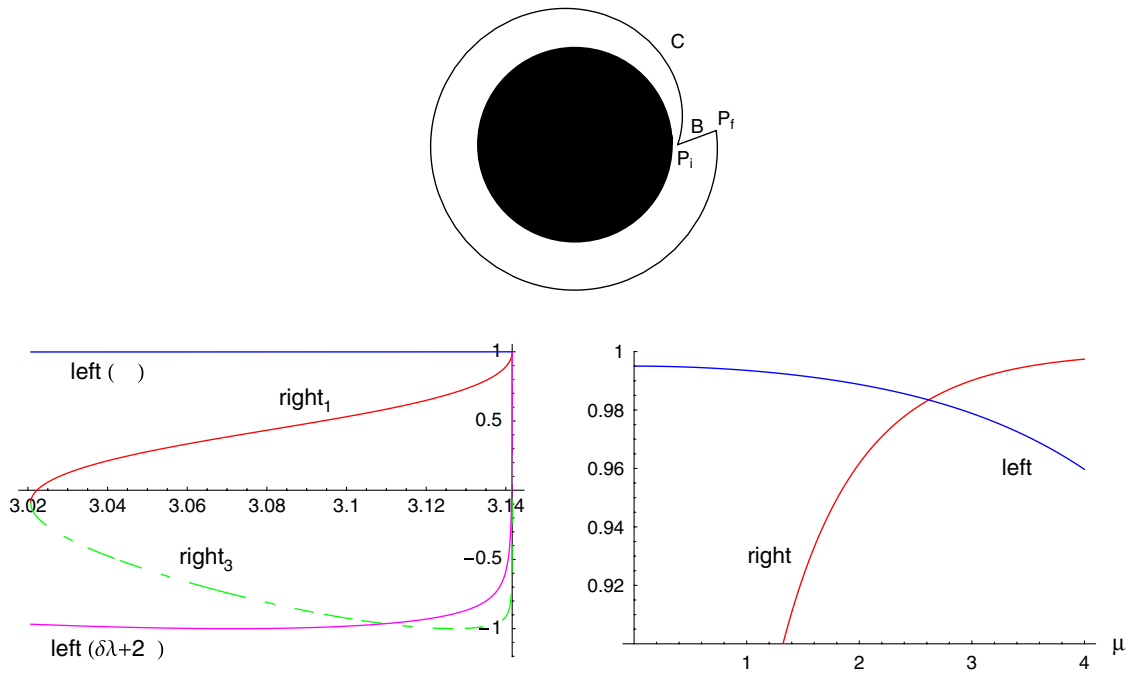


FIG. 9 (color online). Connecting \mathcal{P}_i and \mathcal{P}_f with a type B orbit and a type C winding orbit (winding number $k = 1$); no $k = 0$ type C orbit exists in this case. Left panel: the orbit from \mathcal{P}_i to \mathcal{P}_f of type C. Right panel: the orbit from \mathcal{P}_i to \mathcal{P}_f of type B.

III. CALCULATION OF THE TIME OF FLIGHT

The time of flight for a photon is given by the integral [20]

$$t_{fi} = \pm 2Ma \int_{u_i}^{u_f} \frac{du}{u^2(1-u)\sqrt{a^2 - u^2(1-u)}}. \quad (23)$$

The indefinite integral in the above formula can be expressed in analytic form using elliptic integrals. After considerable algebraic manipulations we obtain the ana-

lytic forms for the three cases of type A, B and C orbits as follows.

Type A

Introduce χ such that [cf. (9f)]

$$u = u_2 - (u_2 - u_3)\cos^2\chi, \quad (24)$$

to obtain

$$t(\chi) = \frac{2an}{u_3^2} \left[\left(1 + u_3 + \frac{n_1^2 - m}{2(m - n_1)(n_1 - 1)} \right) \Pi(n_1; \chi | m) + \frac{u_3^2}{1 - u_3} \Pi(n_2; \chi | m) + \frac{n_1/2}{(m - n_1)(n_1 - 1)} \right. \\ \left. \times \left(E(\chi | m) - \left(1 - \frac{m}{n_1} \right) F(\chi | m) - \frac{n_1 \sin 2\chi \sqrt{1 - m \sin^2 \chi}}{2(1 - n_1 \sin^2 \chi)} \right) \right]. \quad (25)$$

Here E , F and Π are the incomplete elliptic integrals of the first, second and third kinds respectively [25]; u_1, u_2, u_3, m and n are those from (9a)–(9e), and n_1, n_2 are

$$n_1 = 1 - \frac{u_2}{u_3}, \quad (26)$$

$$n_2 = \frac{u_2 - u_3}{1 - u_3}. \quad (27)$$

Types B and C

Introduce χ such that [cf. (12d)]

$$u = u_1 + \frac{1}{n^2} \frac{1 - \cos\chi}{1 + \cos\chi}, \quad (28)$$

to obtain

$$t(\chi) = 2a \left[\frac{\alpha_2(n_1 - 1)}{n_1^2 + m - 2mn_1} \left(\frac{n_1 \sin\chi(k_1 \cos\chi + 1)\sqrt{1 - m \sin^2\chi}}{k_1(1 - n_1 \sin^2\chi)} - E(\chi | m) \right) + \alpha_3(1 - n_2) \left(1 + \frac{1}{k_2} \right) \right. \\ \left. \times \left(\Pi(n_2; \chi | m) + \frac{k_2}{2\sqrt{n_2 - m}} \ln|x_2| \right) + \alpha_1(1 - n_1) \left(1 + \frac{1}{k_1} \right) \left(\Pi(n_1; \chi | m) + \frac{k_1}{2\sqrt{n_1 - m}} \ln|x_1| \right) \right. \\ \left. + F(\chi | m) \left(\frac{\alpha_2}{k_1^2} (1 + (1 + k_1)^2(n_1 - 1)) - \frac{\alpha_1}{k_1} - \frac{\alpha_3}{k_2} \right) \right], \quad (29)$$

where

$$\alpha_1 = \frac{n^3}{n^2 u_1 + 1}, \quad \alpha_2 = \frac{n^5}{(n^2 u_1 + 1)^2}, \quad (30) \\ \alpha_3 = \frac{n^3}{n^2(1 - u_1) - 1},$$

$$k_1 = \frac{1 - u_1 n^2}{1 + u_1 n^2}, \quad k_2 = \frac{1 + (1 - u_1)n^2}{1 - (1 - u_1)n^2}, \quad (31)$$

$$n_1 = \frac{k_1^2}{k_1^2 - 1}, \quad n_2 = \frac{k_2^2}{k_2^2 - 1}, \quad (32)$$

$$x_1 = \frac{\sqrt{n_1 - m} \sin\chi + \sqrt{1 - m \sin^2\chi}}{\sqrt{n_1 - m} \sin\chi - \sqrt{1 - m \sin^2\chi}}, \quad (33)$$

$$x_2 = \frac{\sqrt{n_2 - m} \sin\chi + \sqrt{1 - m \sin^2\chi}}{\sqrt{n_2 - m} \sin\chi - \sqrt{1 - m \sin^2\chi}}. \quad (34)$$

For type B orbits the parameters u_1, m and n are those from

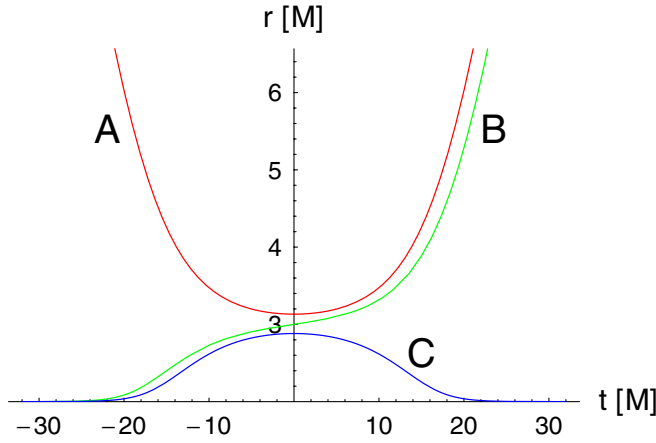


FIG. 10 (color online). Graph $r = r(t)$ in units of M for all three types of orbits. The type A orbit starts at infinity at $t \rightarrow -\infty$, passes the periastron at $t = 0$ and continues to infinity as $t \rightarrow \infty$. The type B orbit starts at the event horizon at $t \rightarrow -\infty$, crosses the critical $r = 3M$ at $t = 0$ and continues to infinity as $t \rightarrow \infty$. The type C orbit starts at the event horizon at $t \rightarrow -\infty$, passes the apastron at $t = M$ and again approaches the event horizon as $t \rightarrow \infty$. In the above example $a = (2/3\sqrt{3}) - 10^{-3}$ for types A and C orbits and $a = (2/3\sqrt{3}) + 5 \times 10^{-4}$ for type B orbit.

(12a)–(12c), while for type C orbits these parameters are from (14a)–(14e).

In Fig. 10 we show examples of $r(t)$ for all three types of orbits. We compared the effectiveness of the analytic method and the pure numerical method to calculate the times of flight. It was found that the algorithm based on the analytic method and implemented with Carlson’s algo-

rithm [31] is always more accurate and 3 to 6 times faster than fourth-order Runge-Kutta integration with adaptive stepsize control.⁴ We also note [29] that it is possible to calculate the time of flight numerically by expanding the integrand (23) into a piecewise rapidly convergent series of analytically integrable functions. Such series easily give results accurate to $10^{-8}M$ for subcritical orbits and are some 6 times faster than the analytic method. The most effective method to calculate the time of flight would thus be a combination of the analytic method for the close to critical orbits and the series solution for the rest.

IV. CONCLUSIONS

In this work we presented the complete solution of the ray-tracing problem in the Schwarzschild spacetime. All the algorithms presented here have been tested for accuracy and for speed of execution and were found to be more accurate and considerably faster than commonly used direct integration methods. We hope that algorithms presented here will be used as a useful tool in solving more complex ray-tracing problems that will elucidate the physics governing complicated transient phenomena in the vicinity of black holes. We would like to remind the community that a similar ray-tracing problem in the Kerr spacetime still remains to be solved.

⁴We note that the algorithm *ellpi* of Numerical Recipes [30] does not give the same results as MATHEMATICA for Π integrals. We rewrote the function *rj* according to Carlson’s original paper [31], and obtained identical results with MATHEMATICA.

- [1] Y. Tanaka *et al.*, Nature (London) **375**, 659 (1995).
- [2] T. Yaqoob, I. M. George, T. J. Turner, K. Nandra, A. Ptak, and P. J. Serlemitsos, *Astrophys. J. Lett.* **505**, L87 (1998).
- [3] C. S. Reynolds, A. C. Fabian, K. Nandra, H. Inoue, H. Kunieda, and K. Iwasawa, *Mon. Not. R. Astron. Soc.* **277**, 901 (1995).
- [4] T. J. Turner, I. M. George, K. Nandra, and R. F. Mushotzky, *Astrophys. J.* **488**, 164 (1997).
- [5] K. Nandra, I. M. George, R. F. Mushotzky, T. J. Turner, and T. Yaqoob, *Astrophys. J.* **477**, 602 (1997).
- [6] C. Fanton, M. Calvani, F. de Felice, and A. Čadež, *Publ. Astron. Soc. Jpn.* **49**, 159 (1997).
- [7] B. C. Bromley, K. Chen, and W. A. Miller, *Astrophys. J.* **475**, 57 (1997).
- [8] Y. Dabrowski and A. N. Lasenby, *Mon. Not. R. Astron. Soc.* **321**, 605 (2001).
- [9] A. Čadež, C. Fanton, and M. Calvani, *New Astron. Rev.* **3**, 647 (1998).
- [10] A. Martocchia, V. Karas, and G. Matt, *Mon. Not. R. Astron. Soc.* **312**, 817 (2000).
- [11] F. K. Baganoff *et al.*, Nature (London) **413**, 45 (2001).
- [12] A. Goldwurm, E. Brion, P. Goldoni, P. Ferrando, F. Daigne, A. Decourchelle, R. S. Warwick, and P. Predehl, *Astrophys. J.* **584**, 751 (2003).
- [13] T. E. Strohmayer, *Astrophys. J. Lett.* **552**, L49 (2001).
- [14] J. M. Miller, A. C. Fabian, R. Wijnands, C. S. Reynolds, M. Ehle, M. J. Freyberg, M. van der Klis, W. H. G. Lewin, C. Sanchez-Fernandez, and A. J. Castro-Tirado, *Astrophys. J. Lett.* **570**, L69 (2002).
- [15] A. Laor, *Astrophys. J.* **376**, 90 (1991).
- [16] V. I. Pariev, B. C. Bromley, and W. A. Miller, *Astrophys. J.* **547**, 649 (2001).
- [17] C. S. Reynolds and M. C. Begelman, *Astrophys. J.* **488**, 109 (1997).
- [18] J. D. Schnittman, eConf C041213:2111 (2004).
- [19] J. D. Schnittman and E. Bertschinger, *Astrophys. J.* **606**, 1098 (2004).
- [20] S. Chandrasekhar, *The Mathematical Theory of Black Holes* (Oxford University Press, New York, 1992).

- [21] K.P. Rauch and R.D. Blandford, *Astrophys. J.* **421**, 46 (1994).
- [22] H. Goldstein, *Classical Mechanics*, Addison-Wesley World Student Series (Addison-Wesley, Reading, MA, 1950).
- [23] W.M. Smart, *Textbook on Spherical Astronomy* (Cambridge University Press, Cambridge, UK, 1965/1971), 5th ed.
- [24] A. Čadež and A. Gomboc, *Astron. Astrophys. Suppl. Ser.* **119**, 293 (1996).
- [25] S. Wolfram, *The Mathematica Book* (Cambridge University Press, Cambridge, UK, 1996), 3rd ed.
- [26] M. Brajnik, B.S. thesis, University of Ljubljana, 1999.
- [27] A. Gomboc, Ph.D. thesis, University of Ljubljana, 2001.
- [28] A. Čadež, M. Brajnik, A. Gomboc, M. Calvani, and C. Fanton, *Astron. Astrophys.* **403**, 29 (2003).
- [29] U. Kostić, B.S. thesis, University of Ljubljana, 2003.
- [30] W.H. Press *et al.*, *Numerical Recipes in C* (Cambridge University Press, Cambridge, UK, 1988).
- [31] B. C. Carlson, *Numer. Math.* **33**, 1 (1979).